PHYSICS OF FLUIDS **27**, 091901 (2015)

The effects of viscosity on the undulatory swimming dynamics of *C. elegans*

M. Backholm,[1] A. K. S. Kasper,[1] R. D. Schulman,[1] W. S. Ryu,[2] and K. Dalnoki-Veress[1,3,a)]

[1]*Department of Physics and Astronomy and the Brockhouse Institute for Materials Research, McMaster University, Hamilton, Ontario L8S 4M1, Canada*
[2]*Department of Physics and the Donnelly Centre, University of Toronto, Toronto, Ontario M5S 1A7, Canada*
[3]*PCT Lab, UMR CNRS 7083 Gulliver, ESPCI ParisTech, PSL Research University, Paris, France*

(Received 22 May 2015; accepted 7 September 2015; published online 29 September 2015)

The undulatory swimming dynamics of the millimetric nematode *Caenorhabditis elegans* was investigated in fluids with different viscosities. The technique of micropipette deflection was used to directly measure the drag forces experienced by the swimming worm in both the lateral and propulsive directions. Gait modulation due to increasing viscosity in our tethered system was found to be qualitatively similar to that of freely swimming worms. Resistive force theory was used to determine the drag coefficients of the slender swimmer, and the experimental values were compared to the classical theories of Lighthill as well as Gray and Hancock. The gait modulation was shown to be independent of how the environmental resistance is changed, indicating the relevance of only the fluid resistance on the swimming kinematics and dynamics of the nematode. © *2015 AIP Publishing LLC*. [http://dx.doi.org/10.1063/1.4931795]

I. INTRODUCTION

Undulatory locomotion is used by crawlers and swimmers, such as snakes and sperm, at length scales spanning almost seven orders of magnitude. In this form of locomotion, the organism moves by propagating waves down its body in an agile and efficient manner. In nature, these slender creatures are forced to adapt to complex environments, such as liquid, sand, and mud.[1] To accomplish this versatility, the organism has two seemingly distinct gaits: crawling on high-friction surfaces[2–4] or through highly viscous fluids,[5] and swimming when immersed in water[6] or sand.[7,8] Understanding the kinematics and dynamics behind the gait transition is an important challenge, and would contribute towards a more general comprehension of the motion of crawlers and swimmers as seen in nature.

The transition between swimming and crawling has been extensively studied with the model organism *C. elegans*,[9–12] a millimetric nematode known for its elegant slithering motion.[13] Interestingly, it has been shown that, instead of transitioning between two distinct gaits, the small worm modulates one single gait continuously as the external resistance is changed.[9,11] Several experimental studies have probed the swimming kinematics of *C. elegans* in different viscosities, finding a decrease in the swimming speed, frequency, and wavelength with an increased fluid viscosity.[5,14,15] Furthermore, in the experimental approach by Yuan *et al.*, the gait modulation of several worms trapped in a channel was studied, and steric confinement interactions were shown to induce gait synchronization between the swimmers.[16] In recent work, the same group studied the kinematics of *C. elegans* nematodes in the presence of fluid flow.[17] By introducing a simple micropipette-based technique, we have recently probed the material properties,[18,19] swimming and crawling dynamics,[20,21] as well as the swimming interactions[22] of *C. elegans*. In addition, we have investigated the swimming dynamics and gait modulation of the nematode close to one and two solid boundaries, where the viscous drag forces

a)Electronic mail: dalnoki@mcmaster.ca

were increased by decreasing the distance to the interface.[23] We found the amplitude and frequency of the worm's swimming to decrease in response to proximity to the boundary.

Given its small size, *C. elegans* has a Reynolds number (Re) slightly less than one in water-like liquids.[20] By studying the decay of fluid velocities away from a swimming nematode in different viscosities, the worm has been shown to indeed behave like a low Re swimmer, or "microswimmer."[15] Microswimmers live in a viscous environment, where inertial effects can be neglected. If, furthermore, assuming no long-ranged hydrodynamic interactions between different body parts of the swimmers, the drag forces they experience as they move can be modelled with restive force theory (RFT).[24,25] According to RFT, the drag forces on a short slender body segment, dl, immersed in a fluid can be related to the segment velocity, v_i, as

$$\mathrm{d}F_\mathrm{T} = -C_\mathrm{T} v_\mathrm{T} \mathrm{d}l, \text{ and } \mathrm{d}F_\mathrm{N} = -C_\mathrm{N} v_\mathrm{N} \mathrm{d}l, \tag{1}$$

where C_i denotes the extrinsic drag coefficient (in units of Pa s) in the normal (i = N) and tangential (i = T) directions along the body. By integrating Eq. (1) along the entire body length, the total drag forces F_N and F_T experienced by the swimmer in the normal and tangential directions can be calculated.

We define the *extrinsic* drag coefficients as $C_i = c_i \eta$, where c_i are the *intrinsic* drag coefficients of the body and η is the fluid viscosity. In order to attain net propulsion, an anisotropy in the environmental resistance is required.[24] This asymmetry is quantified by the ratio of the drag coefficients $K = c_\mathrm{N}/c_\mathrm{T}$. If $K = 1$, no net propulsion is possible for an undulating body in the low Re regime. If $K > 1$, net propulsion will occur in the opposite direction to the waves propagated down the slender body, whereas the converse is true for $K < 1$. Both experiments and theory have determined $K \approx 1.5$ for *C. elegans*,[15,26,27] but only recently have the two intrinsic drag coefficients been directly measured as $c_\mathrm{N} = 5.1 \pm 0.3$ and $c_\mathrm{T} = 3.4 \pm 0.2$ in a water-like buffer.[20]

The magnitude of the two different intrinsic drag coefficients of an undulating body have been theoretically estimated by Gray and Hancock as

$$c_{\mathrm{N,G\&H}} = \frac{4\pi}{\ln(2\lambda/R) + 1/2} \text{ and } c_{\mathrm{T,G\&H}} = \frac{2\pi}{\ln(2\lambda/R) - 1/2}, \tag{2}$$

where R is the radius of the cylindrical body and λ is the swimming wavelength.[6,26,28] Lighthill later improved on this derivation by taking into account hydrodynamic interactions between different segments along the slender body, giving

$$c_{\mathrm{N,L}} = \frac{4\pi}{\ln(0.18\Lambda/R) + 1/2} \text{ and } c_{\mathrm{T,L}} = \frac{2\pi}{\ln(0.18\Lambda/R)}, \tag{3}$$

where Λ is the swimming wavelength as measured along the body.[26] This refined model of Lighthill has been shown to be in excellent agreement with experiments in a buffer with the same viscosity as water.[20] In both of the above described models, a change in the swimming wavelength will result in a small change in the drag coefficients.

The drag coefficients of Eqs. (2) and (3) are derived in the context of an infinite swimmer propagating a sinusoidal wave without a small amplitude restriction. However, the crucial difference arises from the way in which the body is divided into segments of uniform force per unit length. Gray and Hancock equate one wavelength to a segment, which implies that the entire wavelength experiences a constant force. Although this violates an important assumption that this constant force region should be small in comparison to λ, it produced better agreement between experiment and theory. Lighthill refined the expressions of Gray and Hancock by choosing a smaller size for the region of uniform force, and in doing so, produced the resistance coefficients given by Eq. (3). To date, experimental results have been compared to the predictions of both of these models with varying success.[20,23,29–32] Therefore, it is important to continuously test both of these theories to better understand within which circumstance each prediction is more successful and applicable.

In this work, we have investigated the swimming dynamics of *C. elegans* in fluids of different viscosity. By holding the worm by its tail with a force-calibrated micropipette, the drag forces experienced by the worm in the lateral (side to side) and propulsive (forward and backwards) direction were directly measured. Both the kinematics and dynamics of the tail-tethered microswimmer were

analyzed. Using resistive force theory, the drag coefficients were measured and compared to the theoretical models of Lighthill as well as Gray and Hancock. To the best of our knowledge, no previous experimental work has investigated how the intrinsic drag coefficients of *C. elegans* change as the viscosity of the fluid is increased and the swimmer is forced to modulate its gait. We observe a gait modulation induced transition from one model to the other as the viscosity is increased. Furthermore, we show that the gait modulation is independent of the means by which the drag of the system is increased.

II. EXPERIMENTAL METHODS

A. Micropipette deflection

Micropipette deflection was used to investigate the swimming dynamics of single *C. elegans* nematodes in fluids with increasing viscosities. In this technique, the deflection of a long (1–3 cm) and thin (~20 μm) microcapillary is calibrated and used to measure forces with sub-nanonewton resolution. To manufacture the force probes, micropipettes were stretched from glass capillaries with outer and inner diameters of 1 and 0.58 mm (World Precision Instruments) with a pipette puller (Narishige Group PN-30). The end of the pipettes was cut open by looping the capillaries around a hot wire and then quickly quenching the system by turning off the voltage applied across the wire. This rapid cooling causes the glass to solidify and contract, resulting in a sharp cut of the pipette end. The shaping of the pipettes was performed by bending the capillaries over a similar hot wire. The pipettes were calibrated by pushing out a small droplet of water to hang on the outside of the capillary. The pipette and droplet could be imaged with optical microscopy. From the images, the droplet volume, and hence the mass, could be obtained as a function of the pipette deflection, yielding the spring constant. The spring constants of the pipettes used in this work were in the range of 4.6–8.9 nN/μm and the force–deflection was entirely linear in the range used.

To study the swimming dynamics of the worms in both the lateral and propulsive directions, the pipettes were shaped as shown in the schematic illustration of Fig. 1(a). Two short (~200 μm), orthogonal segments of the pipette end were bent in the plane of the swimming motion of the worm. The rest of the pipette was angled at 90° out of the swimming plane to act as a force-sensing cantilever. Here, it is important to note that the deflection of the two shorter segments is negligible in comparison to the long cantilever-part of the pipette. In our swimming experiments, the micropipette was mounted on an xyz-translational stage from above, and placed within a cylindrical chamber, which

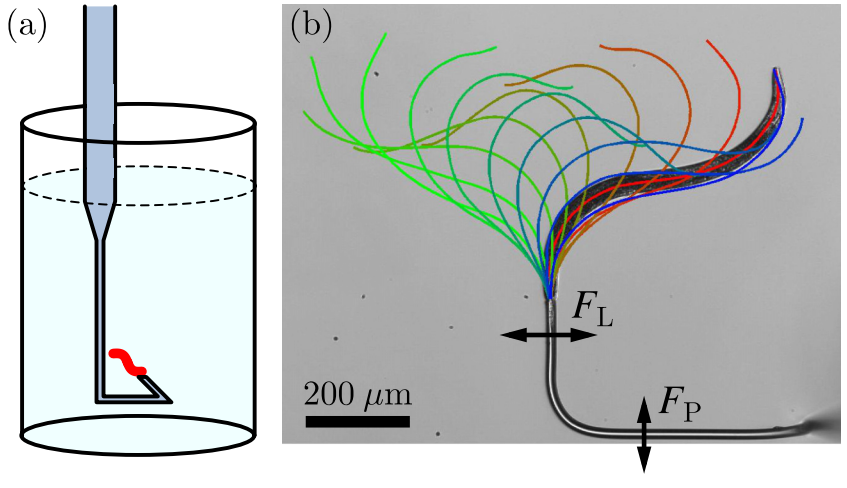

FIG. 1. (a) Schematic diagram (not to scale) of the experimental setup with the force-calibrated micropipette mounted in a cylindrical container. (b) Optical microscopy image of a *C. elegans* nematode caught by its tail. The different lines show a time-lapse of the centreline over one swimming cycle. As the pipette deflects in the two orthogonal directions, the lateral (F_L) and propulsive (F_P) drag forces experienced by the nematode can be directly measured.

was filled with the fluid in which the worms swim. The fluid filled chamber was placed upon the xy translation stage of the inverted microscope so that the region of interest within the chamber as well as the micropipette could always be brought into the field of view.

Before an experiment, tens of worms were picked into a chamber filled with M9 buffer. A nematode was then caught by its tail by applying suction, and left to swim as shown by the optical microscopy image in Figure 1(b). After the measurement in the regular buffer, the same worm, still held by the pipette, was carefully transferred to a new chamber containing a fluid with a different viscosity. The transfer to new chambers was continued until all desired viscosities had been probed. After this, the worm was let go and the same procedure was then repeated by catching a new nematode in the initial chamber. In this way, all higher-viscosity experiments could be compared to the reference swimming behaviour of the same worm in the water-like buffer. We note that in sampling different viscosity environments, care was taken so as to change the order in which the worms were exposed to the different chambers (not simply from lowest to highest) in order to avoid biases.

B. Image analysis

During the experiment, the swimming motion of the worm was followed at 56 fps with a CCD camera (Allied Vision Technologies, GT1660). MATLAB was then used as described in Refs. 20 and 23 to track the motion of the entire nematode body and derive swimming kinematics quantities such as frequency, amplitude, and wavelength. By monitoring the motion of the two orthogonal pipette segments, the lateral (F_L) and propulsive (F_P) drag forces experienced by the nematode were directly measured.

Using the image analysis data, the instantaneous velocity of each segment of the worm's body was calculated. From Eq. (1), we compute the forces acting normal and tangential to this individual body segment, which is then further deconstructed into a lateral and propulsive component. Finally, we numerically integrate each body segment's contribution to find the total lateral and propulsive forces acting on the worm.

C. Viscous solutions

Swimming experiments were performed in M9 solutions with different viscosities. M9 is the standard buffer used for *C. elegans* and consists of various dilute salts required to maintain a suitable osmotic pressure to sustain life.[13] Higher viscosity solutions were achieved by mixing polyethylene oxide (PEO, 10 kg/mol, Sigma-Aldrich) with M9. The molecular weight and polymer combination were selected to ensure a Newtonian fluid behaviour over the range of shear rates relevant to the swimming of the worms as will be shown below. Nematodes were not negatively affected below a PEO mass concentration of 17%. At higher concentrations, worms were seen to either die or stop moving. All experiments in this work were therefore performed at concentrations below 15%.

To obtain fluid viscosities, rheology measurements (MCR301, Anton Paar USA Inc, USA) were performed on five different solutions (mass concentrations of 0%, 1%, 5%, 10%, and 15% PEO in M9). The result is shown in Fig. 2, where the viscosity is plotted as a function of PEO mass concentration (w). The best fit to the data is $\eta(w) = \eta_{H_2O} + 0.099w^{1.8}$ mPa s, where $\eta_{H_2O} = 1$ mPa s is the viscosity of water at 20 °C. This equation was used to calculate all viscosities in this work.

As shown in the inset of Fig. 2, the rheology experiments were performed at shear rates ($\dot{\gamma}$) between 0 and 100 s^{-1} to rule out any shear-thinning flow caused by the dissolved polymers. Since *C. elegans* has been shown[14,33] to use a shear rate within the range of $10 - 20\ s^{-1}$, our polymer solutions can safely be assumed to be Newtonian.

D. *C. elegans* maintenance

Wild-type nematodes (N2) were acquired from the Caenorhabditis Genetics Center and were cultivated on *Escherichia coli* (OP50) nematode growth media (NGM) plates at 20 °C according to standard methods.[34] Only young adult worms were used in the experiments. All chemicals were sourced from Sigma-Aldrich.

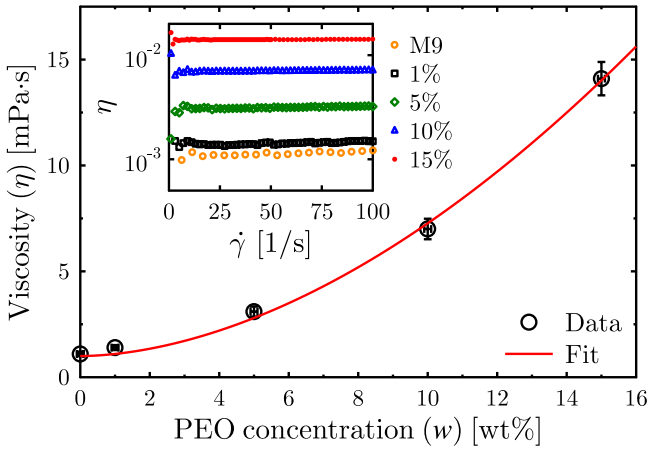

FIG. 2. Viscosity of PEO dissolved in M9 as a function of polymer mass concentration. The line shows the best fit to the data. The error bars correspond to the standard deviation. In the inset, the viscosity is plotted as a function of shear rate ($\dot{\gamma}$) for the five different concentrations.

III. RESULTS AND DISCUSSION

In this section, the kinematics of the tail-tethered worms will first be quantified as the viscosity of the surrounding fluid is increased. Then, the swimming dynamics of the nematodes will be investigated, and the resulting drag coefficients will be compared to the theoretical estimates of Lighthill as well as Gray and Hancock. Finally, the power output will be calculated and the gait modulation will be compared to a previously investigated system wherein the drag forces were increased by introducing nearby solid boundaries.[23]

A. Swimming kinematics

The change in the swimming kinematics of *C. elegans* in increased viscosities is visualized in Fig. 3, where a time-lapse of optical microscopy images of a worm is shown over one swimming cycle (see the supplementary material for movies from the same experiments[35]). A clear decrease in the swimming amplitude (or beating amplitude) is seen. Along the bottom panel of the same figure, the curvature plots from the same experiments as the time-lapse images are shown. In these plots, the swimming curvature is illustrated as a function of time and body coordinate, which defines the position of each segment of the worm's body (head = 0, portion nearest to pipette = 1). To best understand these plots, one should first consider a horizontal line through the graph: the variation of the curvature along this line describes the shape of the worm at that specific point in time. On the other hand, the curvature changes along a vertical line describe the motion of a specific body segment as a function of time. From the curvature plots in Fig. 3, the swimming frequency can be seen to decrease slightly with viscosity (greater temporal spacing between lines of equal curvature), whereas the curvature itself increases (greater range in the intensity associated with the curvature). In Fig. 4(a), the change in swimming frequency compared to that of the M9 buffer ($\Delta f = f_{M9} - f_{\eta}$, where f_{M9} is the swimming frequency of the same worm in M9) is plotted as a function of viscosity. The average swimming frequency in M9 was measured as $f_{M9,ave} = 2.0 \pm 0.2$. The frequency then decreased by around 0.2 Hz between 1 and 4 mPa s, to finally remain stable as the viscosity is further increased. The same change in swimming frequency has been observed for free-swimming worms over the same viscosity range.[14]

As is clear from the time-lapse images in Fig. 3, the swimming amplitude decreases significantly as the viscosity is increased. In Fig. 4(b), the angular amplitude (A_θ) is plotted as a function of viscosity, where the amplitude is defined as half the average total angle swept out by the worm's head in one complete cycle, as shown in the inset. The angular amplitude decreases from around 60° to 15° as the worms modulate their gaits in the different viscosities. The angular amplitude is a convenient

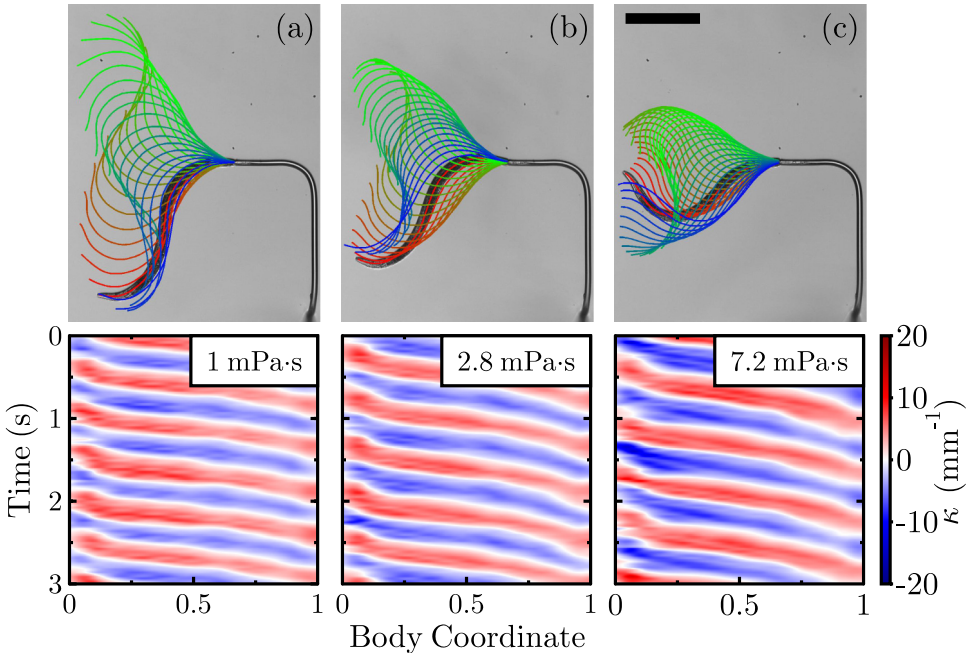

FIG. 3. Time-lapse images (top) of a young adult worm swimming in fluid with viscosities of (a) 1, (b) 2.8, and (c) 7.2 mPa s. The scale bar represents 200 μm. The bottom graphs show the curvature plots for the worms in the top images over several swimming cycles. The body coordinate is defined as the distance along the worm body, where the head is represented by 0 and the tail (portion closest to the pipette) by 1.

metric for the change in the gait of the worm. As will be seen in Section III C, this gait modulation is crucial for the swimmer to maintain its power output at a reasonable level.

To calculate the swimming wavelength of the worm, the curvature plots (exemplified in Fig. 3) were used. By fitting lines to the diagonal high and low curvature regions (i.e., the solid bands) in the graphs, the inverse of the wave speed, v, of the undulatory swimmer can be obtained from the slope.[33] The wavelength along the worm body (i.e., the arc length) can then be calculated as $\Lambda = v/f$, where f is the swimming frequency. In Fig. 4(c), this wavelength has been normalized by the radius (R) of the worm, and is plotted as a function of viscosity. The solid line in the graph shows the best linear fit to the data, which will be used in theoretical calculations in Section III B. If we normalize the wavelength by the length of the worm body outside the pipette (L), we find that it decreases from around $\Lambda/L = 1.2$ to 0.9 in our viscosity range. Due to the tethering of the worms, the swimming wavelength is around 20% lower than for free-swimming worms, but decreases similarly with viscosity.[5] To measure the actual swimming wavelength, λ (as normally defined for a sinusoidal function, rather than the arc-length Λ),

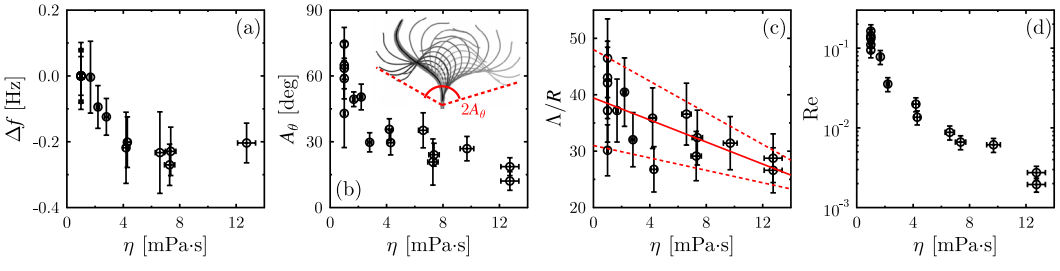

FIG. 4. (a) Change in frequency ($\Delta f = f_{M9} - f_\eta$), (b) angular amplitude (defined as half the average swimming angle, $2A_\theta$, shown in the inset), (c) length-normalized wavelength as measured along the worm body, and (d) the Reynolds number for young adult *C. elegans* nematodes as a function of viscosity. The error bars correspond to the standard deviations from measurements on several swimming cycles of the same worm. The solid line in (c) is the best linear fit to the data: $\Lambda/R = -(1 \mp 0.4)\eta + (39 \pm 8)$, and the dashed lines show the error envelope.

the worm body was modelled as a sine wave at several different points in time. The typical sine wave amplitudes were then approximated and used together with the wavelength measured along the worm body (Λ) to estimate the ordinary wavelength as $\lambda = (0.80 \pm 0.07)\Lambda$. The uncertainty stems from the temporal variations in the shape of the same worm, variations between different worms, as well as the precision of the sine wave fit to the worm centreline.

To classify as a microswimmer, the Reynolds number of the organism needs to be less than unity. The Reynolds number is given by $\mathrm{Re} = \rho l U/\eta$, where ρ and η are the density and dynamic viscosity of the fluid, l is the characteristic length scale, and U is the typical speed. For the case of *C. elegans* in our tethered system, $U \sim 4fL \sin A_\theta$, where f is the swimming frequency, L is the worm length outside the pipette, and A_θ is the angular amplitude, as defined in the inset of Fig. 4(b). The typical length scale in our system can be taken to be the worm radius R. The density (in units of kg/m^3) of the PEO solutions can be calculated using the empirical formula $\rho = 997.07 + 174.41w/100$ (at $T = 298$ K), where w is the percent mass concentration of the polymer and the solvent M9 is approximated as water.[36] The resulting Re is plotted as a function of viscosity in Fig. 4(d) and is shown to decrease by about two orders of magnitude from around 0.15 in M9 to 0.002 in the highest viscosity fluid (~13 mPa s). The low Reynolds number at high viscosities suggests that we can safely describe the swimming of *C. elegans* in these media with low Reynolds number physics. In addition, previous experiments have demonstrated the success of the low Reynolds number model RFT even in M9, where the Reynolds number is large enough that one could worry about the presence of inertial effects.[20,23]

All data points in Fig. 4 are an average over several swimming cycles that are representative of the worm's swimming in general, as observed for several minutes. Each data point corresponds to a single worm.

B. Swimming dynamics

By following the deflection of the micropipette in both orthogonal directions as illustrated in Fig. 1(b), the lateral and propulsive drag forces experienced by the swimming worm were directly measured. In Fig. 5, examples of force versus time data for both the lateral ((a) and (b)) and propulsive ((c) and (d)) directions are shown in a low (left panels) and high (right panels) viscosity fluid. As has been noted in previous work on the swimming dynamics of *C. elegans* in M9,[20] the lateral force is typically twice as large as the propulsive. We see here that this trend persists for the range of viscosities studied. The maximum and minimum force peaks of the lateral force data in Figs. 5(a) and 5(b) occur

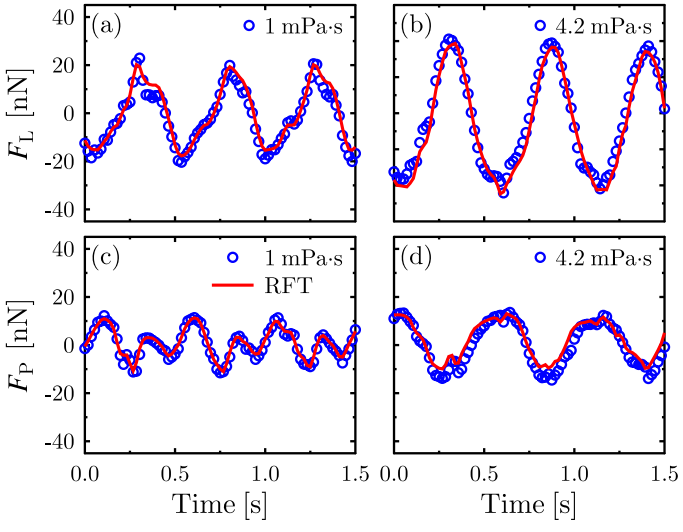

FIG. 5. (a) and (b) Lateral and (c) and (d) propulsive force as a function of time in M9 (left) and a high viscosity fluid (right). The resistive force theory fits are shown with a solid line.

when the worm's body is moving with the highest speed to the right (max) or left (min), whereas the small shoulders on the peaks of the lateral force data in M9 (Fig. 5(a)) arise when the worm's head turns around and starts moving in the opposite direction. As expected, the drag forces increase when the worm is moved to a higher viscosity fluid (Figs. 5(b) and 5(d)). In M9, we measure a mean propulsive force of $\langle F_P \rangle = 0.3 \pm 0.1$ nN,[20] whereas this quantity increases to $\langle F_P \rangle = 3 \pm 2$ nN in fluids with the highest viscosities $\eta = 10 \pm 3$ mPa s. Furthermore, the shoulders in the lateral data disappear as the swimming amplitude decreases and the swimming motion becomes more sinusoidal, as shown in the time-lapse images of Fig. 3. The worm transitions from a high-amplitude swimming in the low viscosity M9 buffer to a more crawling-like wave form in a high viscosity fluid.

As is shown by the solid lines in the graphs of Fig. 5, resistive force theory is successfully fit to the experimental data in both orthogonal directions. As was discussed in our previous work in M9,[20] the success of RFT in capturing the drag force data of *C. elegans* in a water-like buffer is not to be taken for granted, as the young adult nematode has a Re = 0.15, i.e., not very much lower than unity. Therefore, the excellent agreement between RFT and our data indicates that inertial effects can be neglected even for the lowest viscosity studied here. As the Re decreases in higher viscosity fluids, as was shown in Fig. 4(d), the nematode transitions into a more conventional microswimming regime where only viscous forces are relevant.

The extrinsic drag coefficients are fitting parameters for the RFT fits in Fig. 5. Here, we fix the ratio, $K = C_N/C_T = 1.5$, to further constrain the fits. (See Fig. S1 in the supplementary material for a graph of C_N vs. C_T obtained with both drag coefficients as free parameters.[35] The slope in the graph is found to be in good agreement with $K = 1.5$.) Furthermore, a horizontal shift was necessary to make up for a small phase shift (less than $T/20$, where T is the swimming period) between the theory and experimental data.[20] The extrinsic drag coefficients were finally divided by the fluid viscosity, and the resulting intrinsic normal drag coefficient is plotted as a function of viscosity in Fig. 6. Since we hold K constant, we do not show the graph of c_T vs. η here, as the same qualitative trends are seen.

To compare our findings to the theoretical models of Lighthill (Eq. (3)) as well as Gray and Hancock (Eq. (2)), the two different swimming wavelengths (λ and Λ) were first measured as described in Section III A, and normalized with the worm radius (R). These values were entered into the equations to calculate the theoretical drag coefficients, and are plotted as crosses (Lighthill) and squares (Gray and Hancock) in Fig. 6. A linear fit was also made to the Λ/R vs. η data (see Fig. 4(c)), and the resulting empirical function ($\Lambda/R = (-1.0 \mp 0.4)\eta + (39 \pm 8)$) was substituted into the drag coefficient equations, producing the solid lines in Fig. 6. The shaded areas in the graph represent the error regions. Both theoretical models predict a slight *increase* in the intrinsic drag coefficients as the fluid

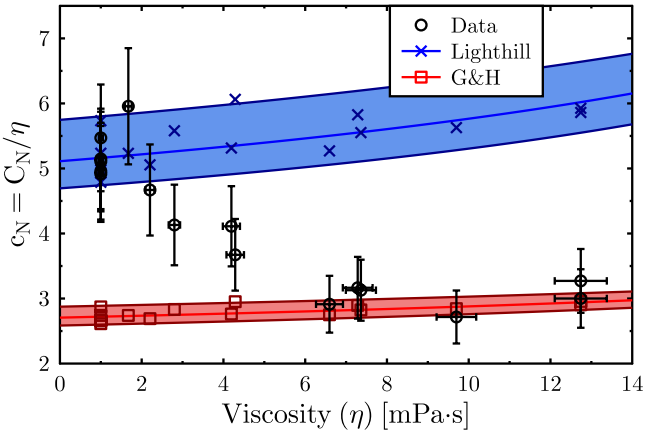

FIG. 6. The intrinsic normal drag coefficient as a function of fluid viscosity. The error bars correspond to the precision of the RFT fits and the error in the spring constant of the pipettes. The cross and square markers represent the theoretical predictions of Lighthill (Eq. (3)) and Gray and Hancock ("G&H," Eq. (2)) evaluated at the wavelengths and viscosities measured for worms as shown in Fig. 4(c). By substituting the empirical function from the linear fit in Fig. 4(c) into the drag coefficient equations, the solid lines in the graph were obtained. The shaded areas represent the error regions. A transition occurs between the two theories as the viscosity is increased.

viscosity is increased. An interesting feature of the results is that there is an unexpected *decrease* in our experimentally determined intrinsic drag coefficients as the external resistance is increased. Moreover, there appears to be a transition between the excellent agreement with the theoretical results of Lighthill at low viscosities, to full agreement with the theory of Gray and Hancock as the viscosity is increased. This significant transition could act to alter the functional dependence of the drag coefficients on the swimming wavelength. The drag coefficients might start to increase with the prediction of Gray and Hancock as the viscosity is increased beyond what was probed in this work.

The transition between the two models is likely due to the gait modulation of the worm. At viscosities above 6 mPa s, the experimental data follow the model developed by Gray and Hancock. In this regime, the worm swimming is more reminiscent of conventional undulatory locomotion of free-swimming worms and the body is less curved onto itself. The predictions of Gray and Hancock (Eq. (2)) are derived in the context of a somewhat coarse grained model. However, their choice of setting the constant force region equal to the wavelength was justified by demonstrating that such a choice produced better agreement with experiments done on freely swimming nematodes. It is, therefore, reasonable that this model succeeds at high viscosities, where the gait-modulating worm has decreased its swimming amplitude significantly, and the worm's motion is more akin to that of a freely swimming worm. On the contrary, Lighthill's refined estimate of the drag coefficients is in excellent agreement with our experimental data in the water-like buffer. In these low-viscosity media, the worm's amplitude is larger and the body is more curved onto itself at times. Therefore, the agreement between Lighthill's theory and our results in this regime might be linked to the fact that Lighthill's theory better accounts for hydrodynamic interactions between body segments. To better understand why this transition occurs would require further theoretical or computational studies specifically considering the swimming within our tail-tethered geometry.

C. Gait modulation

The gait modulation of *C. elegans* occurs to maintain its propulsive thrust whilst sustaining a reasonable power output as the external resistance changes.[5] We have investigated the total power output of the worm, defined as the sum of the viscous power (P_η) exerted on the fluid and the elastic power (P_e) exerted on the bending of the worm body, giving $P_{tot} = P_\eta + P_e$. To calculate the mean viscous power, P_η, we use a similar procedure as for calculating the RFT curves. First, we compute the infinitesimal power expended in overcoming viscous forces for each body segment $dF_T v_T + dF_N v_N$, where dF_N and dF_T are given in Eq. (1). Subsequently, this quantity is numerically integrated over the entire body of the worm to find the total power. The mean bending power was calculated as

$$P_e = \frac{EILf\langle\kappa^2\rangle}{2}, \tag{4}$$

where L is the worm length outside of the pipette, $\langle\kappa^2\rangle$ is the mean square body curvature, f is the swimming frequency, and $EI = (1.2 \pm 0.7) \cdot 10^{-14}$ N m^2 is the bending stiffness for young adult worms obtained from direct bending measurements performed with micropipette deflection.[18]

Calculating the power components as above, we find that both components are constant within experimental error over the viscosity range probed in this work (see Fig. S5 in the supplementary material for a graph of the mean viscous and elastic power as a function of viscosity[35]). The average for all young adult worms is $P_\eta = 0.41 \pm 0.15$ nW and $P_e = 0.14 \pm 0.03$ nW, which sums up to a total power output of $P_{tot} = 0.55 \pm 0.18$ nW. The elastic bending power calculated here deviates from that calculated by Fang-Yen *et al.*[5] ($P_e \approx 4$ nW) due to a higher estimation of the bending stiffness in their work ($EI = (9.5 \pm 1.0) \cdot 10^{-14}$ N m^2). The constant power output, as has also been reported by Fang-Yen *et al.*, demonstrates that the worm actively changes its swimming motion to maintain the same level of energy consumption in different environments. This ability is thought to be crucial for the nematode to move through and survive in continuously changing surroundings of, e.g., water, mud, and soil.[9] If not capable of modulating its gait when moving into a region of increased resistance, the nematode would have to increase its power output to maintain the same swimming or crawling waveform, and in that way risk exhaustion and even starvation.

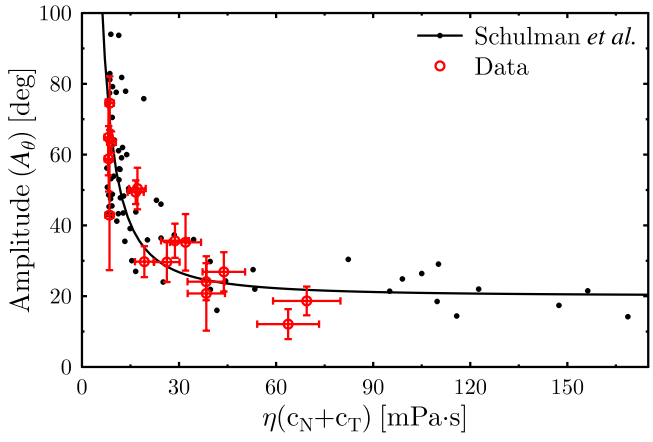

FIG. 7. Angular amplitude (circles) as a function of the sum of the extrinsic drag coefficients. The error bars correspond to the standard deviations from measurements on several swimming cycles of the same worm. The dots are data from Schulman *et al.*,[23] where one and two solid boundaries were brought close to the swimming nematode to enhance the drag experienced by the worm. The solid line is included to guide the eye.

In previous studies, the kinematics of *C. elegans* has been investigated by chemically altering the surrounding fluid, making it more viscous,[5,14,15,33] viscoelastic,[37] or shear-thinning.[38] In our previous work,[23] we enhanced the drag forces experienced by tail-tethered swimming nematodes by holding them close to one solid boundary, or confined between two surfaces. In Fig. 7, the angular amplitude measured in that work (defined in the same way as shown in the inset of Fig. 4(b)) is plotted as a function of the sum of the two extrinsic drag coefficients, $C_N + C_T = \eta(c_N + c_T)$. In the same graph, the results of our present study are plotted (circles). Evidently, the gait modulation of the worm is identical within a chemically altered fluid compared with a fluid where the drag forces have been enhanced by changing the physical geometry of the system. The kinematics of the nematode is, in other words, affected solely by the change in its extrinsic drag coefficients. By using different mutants, future studies could investigate the effect of, e.g., mechanosensation on the gait modulation of *C. elegans* to probe the biological reasons governing the change in swimming kinematics with increased external resistance.

IV. SUMMARY AND CONCLUSIONS

Here, we have used the technique of micropipette deflection to probe the undulatory swimming dynamics of the nematode *C. elegans* in fluids with different viscosities. The change in the kinematics of the tail-tethered worm was quantified, and the swimmer was shown to move with a decreased frequency, amplitude, and wavelength as the fluid viscosity was increased. The drag forces experienced by the worm in the lateral and propulsive directions were directly measured over time, and resistive force theory was used to derive the drag coefficients of the microswimmer. The intrinsic drag coefficients were, surprisingly, shown to transition between the classical models of Lighthill at low viscosities to that of Gray and Hancock at high viscosities. This transition was attributed to the gait modulation of the nematode, adapting from a large-amplitude motion, to a more conventional, small-amplitude undulatory motion. A deeper theoretical treatment of the system would be of future interest to investigate the effects of gait modulation on the intrinsic drag coefficients of an undulatory microswimmer. Furthermore, experimental studies of the swimming dynamics at higher viscosities would shed more light on whether the intrinsic drag coefficients continue to follow the estimates of Gray and Hancock in the low-amplitude swimming regime.

Finally, the total power output of the nematode was found to remain constant as the environmental resistance changed. That is, the worm modulates its gait to increase propulsion without modifying its power expenditure. The gait modulation was shown to be independent of how the viscous forces of the system are enhanced, indicating that only the hydrodynamic forces of the system influence the undulatory locomotion kinematics and dynamics of the nematode.

ACKNOWLEDGMENTS

The authors thank Adam Fortais and Dr. John de Bruyn for assisting with the viscosity measurements. The financial support by Natural Science and Engineering Research Council of Canada (Discovery Grant) is gratefully acknowledged.

[1] E. Lauga, "The bearable gooeyness of swimming," J. Fluid Mech. **762**, 1–4 (2014).
[2] E. Niebur and P. Erdős, "Theory of the locomotion of nematodes: Dynamics of undulatory progression on a surface," Biophys. J. **60**, 1132–1146 (1991).
[3] Z. V. Guo and L. Mahadevan, "Limbless undulatory propulsion on land," Proc. Natl. Acad. Sci. U. S. A. **105**, 3179–3184 (2008).
[4] D. L. Hu, J. Nirody, T. Scott, and M. J. Shelley, "The mechanics of slithering locomotion," Proc. Natl. Acad. Sci. U. S. A. **106**, 10081–10085 (2009).
[5] C. Fang-Yen, M. Wyart, J. Xie, R. Kawai, T. Kodger, S. Chen, Q. Wen, and A. D. T. Samuel, "Biomechanical analysis of gait adaptation in the nematode *Caenorhabditis elegans*," Proc. Natl. Acad. Sci. U. S. A. **107**, 20323–20328 (2010).
[6] J. Gray and G. J. Hancock, "The propulsion of sea-urchin spermatozoa," J. Exp. Biol. **32**, 802–814 (1955), see http://jeb.biologists.org/content/32/4/802.abstract.
[7] R. D. Maladen, Y. Ding, C. Li, and D. I. Goldman, "Undulatory swimming in sand: Subsurface locomotion of the sandfish lizard," Science **325**, 314–317 (2009).
[8] Y. Ding, S. S. Sharpe, A. Masse, and D. I. Goldman, "Mechanics of undulatory swimming in a frictional fluid," PLoS Comput. Biol. **8**, e1002810 (2012).
[9] S. Berri, J. H. Boyle, M. Tassieri, I. A. Hope, and N. Cohen, "Forward locomotion of the nematode *C. elegans* is achieved through modulation of a single gait," HFSP J. **3**, 186–193 (2009).
[10] J. T. Pierce-Shimomura, B. L. Chen, J. J. Mun, R. Ho, R. Sarkis, and S. L. McIntire, "Genetic analysis of crawling and swimming locomotory patterns in *C. elegans*," Proc. Natl. Acad. Sci. U. S. A. **105**, 20982–20987 (2008).
[11] J. H. Boyle, S. Berri, M. Tassieri, I. A. Hope, and N. Cohen, "Gait modulation in *C. elegans*: It's not a choice, it's a reflex!," Front. Behav. Neurosci. **5**, 10 (2011).
[12] J. H. Boyle, S. Berri, and N. Cohen, "Gait modulation in *C. elegans*: An integrated neuromechanical model," Front. Comput. Neurosci. **6**, 10 (2012).
[13] B. Wood, *The Nematode Caenorhabditis Elegans* (Cold Spring Harbor Laboratory Press, New York, 1988).
[14] J. Sznitman, X. Shen, P. K. Purohit, and P. E. Arratia, "The effects of fluid viscosity on the kinematics and material properties of *C. elegans* swimming at low Reynolds number," Exp. Mech. **50**, 1303–1311 (2010).
[15] J. Sznitman, X. Shen, R. Sznitman, and P. E. Arratia, "Propulsive force measurements and flow behavior of undulatory swimmers at low Reynolds number," Phys. Fluids **22**, 121901 (2010).
[16] J. Yuan, D. M. Raizen, and H. H. Bau, "Gait synchronization in *Caenorhabditis elegans*," Proc. Natl. Acad. Sci. U. S. A. **111**, 6865–6870 (2014).
[17] J. Yuan, D. M. Raizen, and H. H. Bau, "Propensity of undulatory swimmers, such as worms, to go against the flow," Proc. Natl. Acad. Sci. U. S. A. **112**, 3606–3611 (2015).
[18] M. Backholm, W. S. Ryu, and K. Dalnoki-Veress, "Viscoelastic properties of the nematode *Caenorhabditis elegans*, a self-similar, shear-thinning worm," Proc. Natl. Acad. Sci. U. S. A. **110**, 4528–4533 (2013).
[19] M. Backholm, W. S. Ryu, and K. Dalnoki-Veress, "The nematode *C. elegans* as a complex viscoelastic fluid," Eur. Phys. J. E **38**, 36 (2015).
[20] R. D. Schulman, M. Backholm, W. S. Ryu, and K. Dalnoki-Veress, "Dynamic force patterns of an undulatory microswimmer," Phys. Rev. E **89**, 050701 (2014).
[21] Y. Rabets, M. Backholm, K. Dalnoki-Veress, and W. S. Ryu, "Direct measurements of drag forces in *C. elegans* crawling locomotion," Biophys. J. **107**, 1980–1987 (2014).
[22] M. Backholm, R. D. Schulman, W. S. Ryu, and K. Dalnoki-Veress, "Tangling of tethered swimmers: Interactions between two nematodes," Phys. Rev. Lett. **113**, 138101 (2014).
[23] R. D. Schulman, M. Backholm, W. S. Ryu, and K. Dalnoki-Veress, "Undulatory microswimming near solid boundaries," Phys. Fluids **26**, 101902 (2014).
[24] N. Cohen and J. H. Boyle, "Swimming at low Reynolds number: A beginners guide to undulatory locomotion," Contemp. Phys. **51**, 103–123 (2010).
[25] E. Lauga and T. R. Powers, "The hydrodynamics of swimming microorganisms," Rep. Prog. Phys. **72**, 096601 (2009).
[26] J. Lighthill, "Flagellar hydrodynamics–The John von Neumann lecture, 1975," SIAM Rev. **18**, 161–230 (1976).
[27] J. Gray and H. W. Lissmann, "The locomotion of nematodes," J. Exp. Biol. **41**, 135–154 (1964), see http://jeb.biologists.org/content/41/1/135.
[28] J. Gray, "Undulatory propulsion," Q. J. Microsc. Sci. **94**, 551–578 (1953), see http://jcs.biologists.org/content/s3-94/28/551.
[29] J. Sznitman, P. K. Purohit, P. Krajacic, T. Lamitina, and P. E. Arratia, "Material properties of *Caenorhabditis elegans* swimming at low Reynolds number," Biophys. J. **98**, 617–626 (2010).
[30] B. Friedrich, I. Riedel-Kruse, J. Howard, and F. Jülicher, "High-precision tracking of sperm swimming fine structure provides strong test of resistive force theory," J. Exp. Biol. **213**, 1226–1234 (2010).
[31] P. Bayly, B. Lewis, E. Ranz, R. Okamoto, R. Pless, and S. Dutcher, "Propulsive forces on the flagellum during locomotion of *Chlamydomonas reinhardtii*," Biophys. J. **100**, 2716–2725 (2011).
[32] B. Rodenborn, C.-H. Chen, H. L. Swinney, B. Liu, and H. P. Zhang, "Propulsion of microorganisms by a helical flagellum," Proc. Natl. Acad. Sci. U. S. A. **110**, E338–E347 (2013).
[33] J. Korta, D. A. Clark, C. V. Gabel, L. Mahadevan, and A. D. T. Samuel, "Mechanosensation and mechanical load modulate the locomotory gait of swimming *C. elegans*," J. Exp. Biol. **210**, 2383–2389 (2007).

[34] S. Brenner, "The genetics of *Caenorhabditis elegans*," Genetics **77**, 71–94 (1974), see http://www.genetics.org/content/77/1/71.abstract.
[35] See supplementary material at http://dx.doi.org/10.1063/1.4931795 for information about the RFT fits performed with a free drag coefficient ratio, for movies of a worm swimming in different viscosities, and for a graph of the power output as a function of fluid viscosity.
[36] P. Gonzalez-Tello, F. Camacho, and G. Blazquez, "Density and viscosity of concentrated aqueous solutions of Polyethylene Glycol," J. Chem. Eng. Data **39**, 611–614 (1994).
[37] X. N. Shen and P. E. Arratia, "Undulatory swimming in viscoelastic fluids," Phys. Rev. Lett. **106**, 208101 (2011).
[38] D. A. Gagnon, N. C. Keim, and P. E. Arratia, "Undulatory swimming in shear-thinning fluids: Experiments with *Caenorhabditis elegans*," J. Fluid Mech. **758**, R3 (2014).